Examination of the Effect of Concrete Crosstie Rail Seat Deterioration on Rail Seat Load Distribution

Matthew J. Greve, Marcus S. Dersch, J. Riley Edwards, Christopher P. L. Barkan, Hugh Thompson, Theodore R. Sussmann, Jr., and Michael T. McHenry

One of the more critical failure modes of concrete crossties in North America is the degradation of the concrete surface at the crosstie rail seat, also known as rail seat deterioration (RSD). Loss of material beneath the rail can lead to wide gage, cant deficiency, reduced clamping force of the fastening system, and an increased risk of rail rollover. Previous research conducted at the University of Illinois at Urbana–Champaign (UIUC) identified five primary failure mechanisms associated with RSD: abrasion, crushing, freeze–thaw damage, hydroabrasive erosion, and hydraulic pressure cracking. Because the magnitude and distribution of load applied to the rail seat affects four of these five failure mechanisms, effectively addressing RSD requires an understanding of the factors affecting rail seat load distribution. As part of a larger study aimed at improving concrete crossties and fastening systems, UIUC researchers are attempting to characterize the loading environment at the rail seat by using matrix-based tactile surface sensors (MBTSS). This instrumentation technology has been implemented in both laboratory and field environments and has provided valuable insight into the distribution of a single load over consecutive crossties. This paper focuses on the analysis of data gathered from MBTSS experiments designed to explore the effect of manufactured RSD on the load distribution and pressure magnitude at the rail seat. The knowledge gained from these experiments will be integrated with associated research conducted at UIUC to form the framework for a mechanistic design approach for concrete crossties and fastening systems.

As the demand in North America for high-performance, low-maintenance railroad infrastructure has increased, the use of concrete crossties and elastic fastening systems has grown. One of the performance failures associated with concrete crossties is the degradation of the concrete material directly below the rail, in the area of the crosstie known as the rail seat. This degradation is commonly referred to as rail seat deterioration (RSD), or rail seat abrasion. Figure 1 illustrates a typical instance of severe RSD, with the depth of wear increasing toward the field side of the rail seat. RSD has become a problematic failure for concrete crossties since it was first observed in the 1980s; it is often found in regions of steep grades, high curvature, and the presence of moisture (*1*). If left untreated, RSD may lead to accelerated wear of the fastening system, wide gage, excessive rail cant, and an increased risk of derailment caused by rail rollover (*1*).

According to a recent survey of North American railroad industry experts, RSD was ranked as the most critical problem with concrete crossties and fastening systems (*2*). It was also ranked as the concrete crosstie and fastening system topic most in need of research (*2*). Researchers at the University of Illinois at Urbana–Champaign (UIUC) are investigating common concrete crosstie and fastening system failure modes, such as flexural cracking, shoulder failure, and system fatigue, and are using their findings to guide a proposed framework for a mechanistic design process. This design process would establish a clearer procedure for the design of crossties and fastening systems, resulting in fewer service failures and higher reliability of the track structure and its components (*3*). Among the crosstie and fastening system failures investigated by researchers at UIUC are the failure modes that result in RSD. Previous research identified five feasible failure mechanisms by which RSD is formed: abrasion, crushing, freeze–thaw cracking, hydroabrasive erosion, and hydraulic pressure cracking (*1*). Of these five failure mechanisms, four are affected by the loading environment at the crosstie rail seat; the exception is freeze–thaw cracking. Hence, UIUC researchers have undertaken an effort to better understand the distribution of the rail seat load and its effect on RSD. Previous research highlighted the effect of rail pad modulus, fastening system type, and loading environment on the rail seat load distribution (*4, 5*).

INSTRUMENTATION TECHNOLOGY

To characterize the distribution of load at the rail seat, UIUC researchers used matrix-based tactile surface sensors (MBTSS). The MBTSS system used by UIUC is manufactured by Tekscan and consists of rows and columns of conductive ink that, when pressed together by a load applied normally to the contact plane, output a change in resistivity at each intersection of a row and a column. The output, called the raw sum, can be interpreted as the pressure exerted on the sensor at an intersection given the total applied load. The MBTSS system simultaneously outputs the area over which

M. J. Greve, M. S. Dersch, J. R. Edwards, and C. P. L. Barkan, Rail Transportation and Engineering Center, Department of Civil and Environmental Engineering, University of Illinois at Urbana–Champaign, 205 North Mathews Avenue, Urbana, IL 61801. H. Thompson, Federal Railroad Administration, 1120 Vermont Avenue NW, Washington, DC 20005. T. R. Sussmann, Jr., John A. Volpe National Transportation Systems Center, 55 Broadway, Cambridge, MA 02142. M. T. McHenry, Association of American Railroads, Transportation Technology Center, Inc., 55500 DOT Road, Pueblo, CO 81001. Corresponding author: M. J. Greve, greve1@illinois.edu.

Transportation Research Record: Journal of the Transportation Research Board, No. 2476, Transportation Research Board, Washington, D.C., 2015, pp. 1–7.
DOI: 10.3141/2476-01

FIGURE 1 Typical wear pattern of severe RSD.

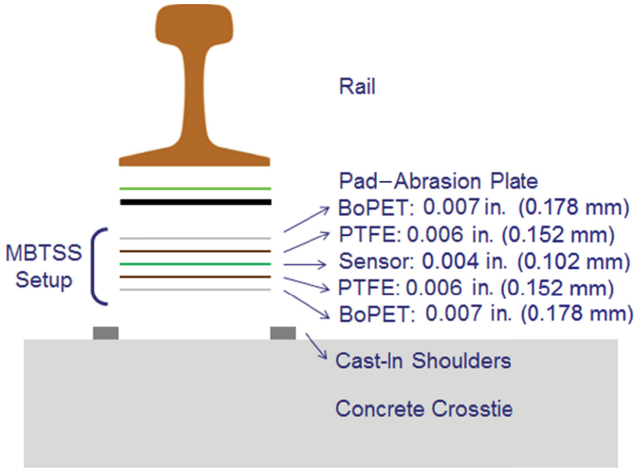

FIGURE 2 MBTSS layers and thicknesses (*6*) (BoPET = biaxially oriented polyethylene terephthalate; PTFE = polytetrafluoroethylene).

this load is applied. This is called the contact area of the load and is calculated from the number of sensing locations that indicate an applied load. Data are collected from the entire sensing area at a maximum rate of 100 Hz. A known or assumed input load is used to calibrate the data during analysis.

Previous experimentation at the University of Kentucky and UIUC showed that MBTSS are susceptible to shear and puncture damage. To protect the sensors, layers of biaxially oriented polyethylene terephthalate and polytetrafluoroethylene are secured to both sides of a sensor that has been trimmed to fit the rail seat. The assembly is then installed between the rail pad assembly and the concrete crosstie rail seat (Figure 2) (*6*).

EXPERIMENTATION PLAN

Field experimentation was conducted at the Transportation Technology Center (TTC), Inc., in Pueblo, Colorado. Untreated concrete crosstie rail seats, one per crosstie, were ground to simulate common RSD wear profiles and then installed in a section of a service track that is a part of the Facility for Accelerated Service Testing. All three sections were tamped after installation of the crossties in 2013 and had experienced less than 1 million gross tons of traffic between tamping and the date of the experiment. When testing was not being conducted, steel plates were inserted on the worn rail seats to restore the original cant. The crossties were arranged in three sections of 20 crossties, each section having a specified target wear depth. The wear depth was gradually increased from both ends of each section until the target depth was achieved at the center of the section. Figure 3 illustrates the wear depth profile of each section; the target wear depth of Section 1 was ¼ in. (6.35 mm), the target wear depth of Section 2 was ⅜ in. (9.53 mm), and the target wear depth of Section 3 was ¾ in. (19.05 mm). Section 1 was located in a section of tangent track, and Sections 2 and 3 were located in 8.9° (195-m) and 3.9° (445-m) curves, respectively, with the ground rail seats installed on the high rail of the curve. The rail seats of each section were ground to specific wear profiles, as illustrated in Figure 4. Rail seats in Section 1 were ground to a uniform wear depth (emulating RSD typically associated with tangent track), preserving the design cant of the rail seat of 1:40 (Figure 4*a*). Rail seats in Sections 2 and 3 were ground to simulate triangular wear across the entire rail seat (emulating reverse rail cant), beginning from the original plane of the rail seat at the gage side shoulder and increasing to the prescribed

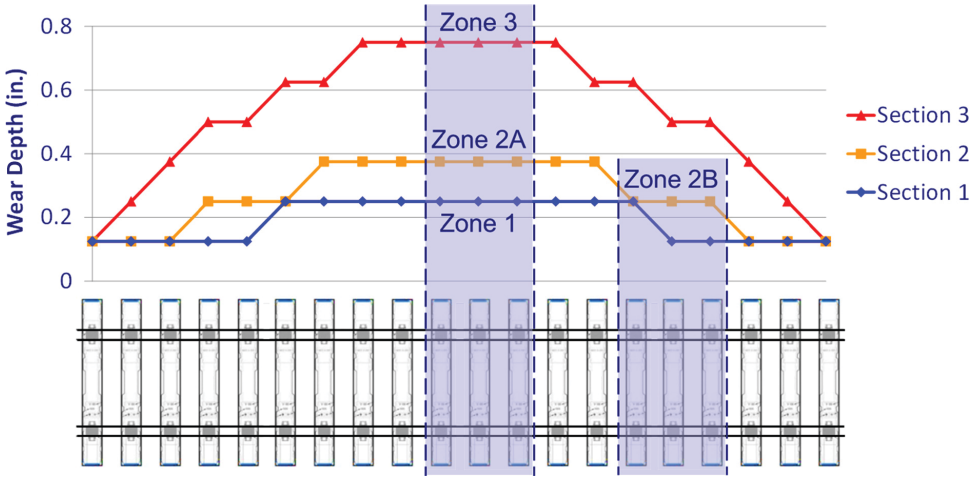

FIGURE 3 Wear depth profiles and location of instrumentation zones.

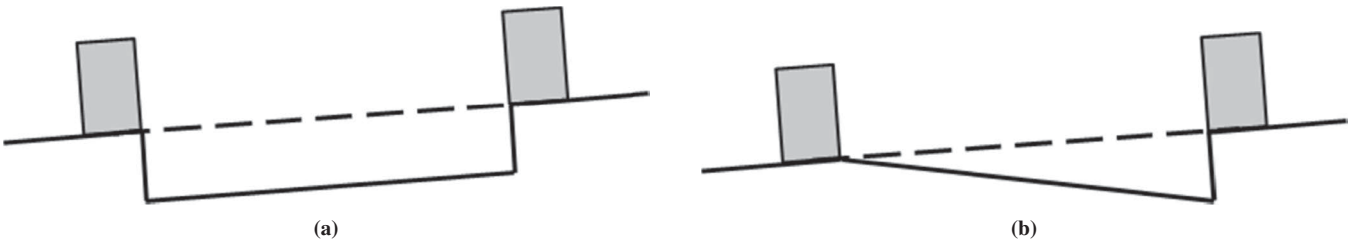

FIGURE 4 Illustration of rail seat wear profiles: (*a*) uniform wear (Section 1) and (*b*) triangular wear (Sections 2 and 3).

wear depth at the field side shoulder (Figure 4*b*). The Safelok I fastening system was used for all three sections.

Four instrumentation zones were chosen, as shown in Figure 3, to capture all three target wear depths (Zones 1, 2A, and 3). Additionally, a fourth zone (Zone 2B) was chosen in Section 2 at a wear depth of ¼ in. This was the same wear depth as Zone 1 and was chosen to isolate the effect of the rail seat wear profile (uniform or triangular) on rail seat load distribution. Each instrumentation zone comprised three instrumented rail seats. Each rail seat was instrumented with MBTSS to capture the rail seat load distribution, as well as with linear potentiometers to capture the rail base vertical displacement on both the field and the gage side of the rail. The potentiometers were mounted on displacement fixtures attached to the crosstie with anchored screws and were used to calculate rail base rotation.

Loads were applied to the track structure with the FRA T-18 gage restraint measurement vehicle. The vehicle is designed to evaluate the health of crossties and fastening systems by using a gage restraint measurement system (GRMS), a deployable axle that can be used to apply controlled vertical and lateral loads to the track structure (*7*). Testing consisted of both static and dynamic load application at each zone. The vertical wheel load was kept constant at 20,000 lbf (89 kN), comparable to the wheel loads of Amtrak long-distance passenger equipment, for all static and dynamic experiments. The lateral wheel load was varied to generate lateral-vertical (L/V) force ratios ranging from 0 to 0.8. For static experiments, the L/V force ratio was increased at 0.2 increments; for dynamic experiments, the L/V force ratio was increased at 0.4 increments. Dynamic experiments were conducted at 5 and 15 mph (8 and 24 km/h).

To obtain a control case, the results from this experimentation were compared with data gathered at TTC as part of an earlier experimentation effort (*5*). The control rail seats were untreated and the original rail seat geometry was intact; the rail sets were tested in tangent track on TTC's railroad test track. The control experiments were conducted at 20,000 lbf vertical wheel load with increasing lateral loads, such that the L/V force ratios applied to the track structure ranged from 0 to 0.6.

RESULTS OF EXPERIMENTATION

To guide the analysis of the data, several hypotheses were generated that characterized the loading environment and the effect of RSD. These hypotheses can be broken into three primary areas: the effect of the rail seat wear profile, comparison of static and dynamic loading environments, and characterization of the loading environment by rail roll.

To achieve triangular rail seat wear profiles of increasing depth at the field side of the rail seat, the slope of the worn profile must increase. Because of this increase, the toe load applied to the rail base by the field side clips will be reduced, and the rail will be able to rotate more freely. As the rail rotates toward the field, increasing the negative rail cant, the area of the rail seat engaged in load transfer will be reduced. Hence, it is hypothesized that the contact area will be reduced by an increase in the wear depth of a triangular rail seat wear profile. This loss of contact area will inherently result in increased average pressures, and it is hypothesized that the maximum pressures exerted in each instrumentation zone will also be increased.

Associated experimentation on concrete crossties and fastening systems at UIUC has shown that an increase in train speed tends to decrease vertical deflection of the rail relative to the crosstie (*8*). In these cases, static load application serves as the upper bound of deflection. It is theorized that at higher speeds, the track structure does not have time to settle completely after each load application, as it does under static loads. It is hypothesized that this behavior will be mirrored by the contact area and that an increase in speed will then yield a decrease in contact area, regardless of rail seat wear profile.

So that the findings of this experimentation would be applicable to industry use, an effort was made to correlate the rail seat load distribution to a parameter that could be measured by track geometry cars such as the T-18. Of the geometry data gathered by the T-18, rail cant was identified as the parameter most directly affecting the rail seat load distribution. Hence it was determined that the linear correlation between maximum pressure and rail cant should yield an R^2 value of 0.8 or higher for it to be considered a reliable relationship.

Effect of Rail Seat Wear Profile

Figure 5 shows the qualitative effect of wear depth on the rail seat load distribution under static load application. In the figure, all rail seats are oriented so that the field side of the rail seat is toward the top of the page. As wear depth increases from left to right across the figure, the severity of load concentration on the field side of the rail seat increases, indicating reduced contact areas and higher contact pressures. As predicted by the hypothesis, a significant reduction in contact area from ⅜-in. to ¾-in. triangular wear can be observed.

The qualitative effect of increased L/V force ratio of the applied static load on the rail seat load distribution is presented in Figure 6. In this figure, the vertical load and rail seat wear profile are held constant as the L/V force ratio varies. At low L/V, the rail seat load tends to distribute over a portion of the rail seat on both the gage and field sides. Most of the rail seat wear profiles exhibit consistent behavior. As the rail rotates under an increasing L/V force ratio, the rail pad deforms under the rail base, distributing a reduced portion of the rail seat load on the gage side. At L/V force ratios higher than 0.4, the rail continues to rotate, disengaging the gage side of the rail seat entirely and concentrating the load across the entire width of the field side. It is hypothesized that a critical point of rotation is exceeded

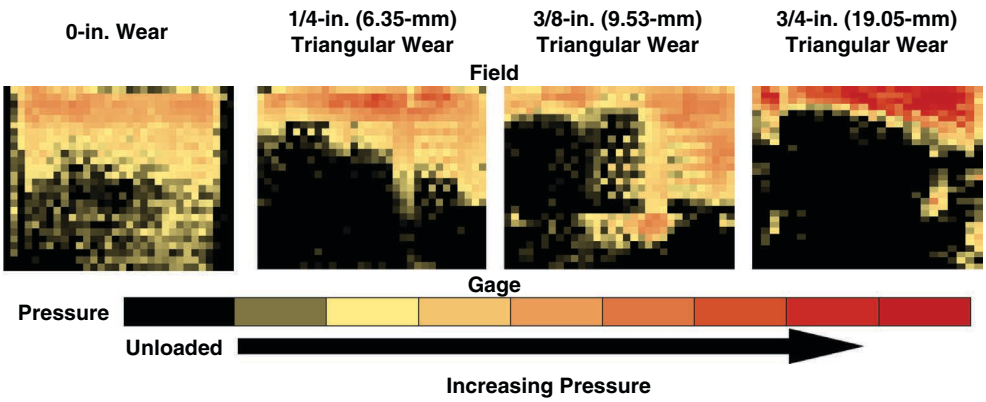

FIGURE 5 Rail seat load distribution under increasing wear depth; 20,000-lbf (89 kN) vertical wheel load and 0.6 L/V force ratio.

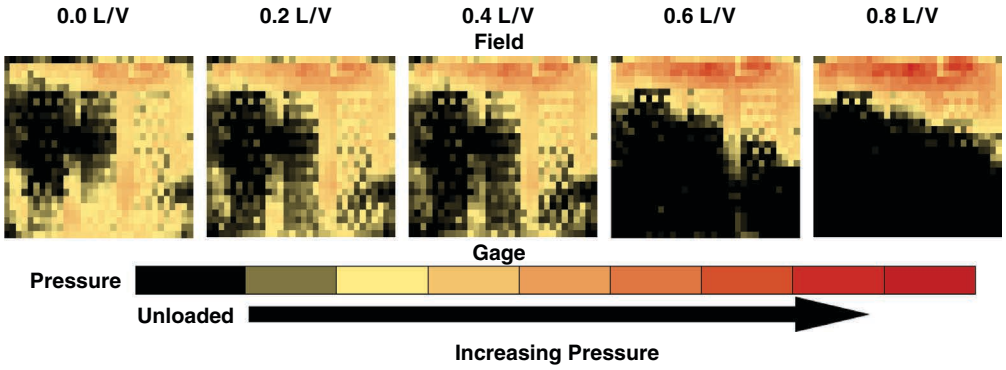

FIGURE 6 Rail seat load distribution under increasing L/V force ratio; 20,000-lbf (89 kN) vertical wheel load, 1/4-in. triangular wear.

at 0.6 L/V, at which the vertical wheel load no longer provides a moment resisting the tendency of the rail to roll to the field.

The reduction of contact area shown in Figures 5 and 6 is quantified in Figure 7, which shows the effect of an increased L/V force ratio for all instrumentation zones at a constant vertical load. Error bars in Figure 7 show plus or minus one standard deviation from the average for each rail seat wear profile. Most of this variability is caused by differences in the initial contact area of each rail seat within a given instrumentation zone at 0 L/V, and the relative behavior is consistent in each zone. The visual trend of reduced contact area in zones of greater wear depth is quantified in Figure 7, and the contact area resulting from ⅜-in. wear is consistently 75% larger than that resulting from ¾-in. wear. The effect of rail seat wear profile is also quantified in Figure 8, which shows that the average contact area resulting from ¼-in. uniform wear is 43% less than that resulting from ¼-in. triangular wear below an L/V force ratio of 0.6. It is hypothesized that this difference is caused by reduced deflection of the clip toes, leading to reduced clamping force applied to the rail base, which allows the rail to rotate more freely, leading to less contact between the rail base and rail pad.

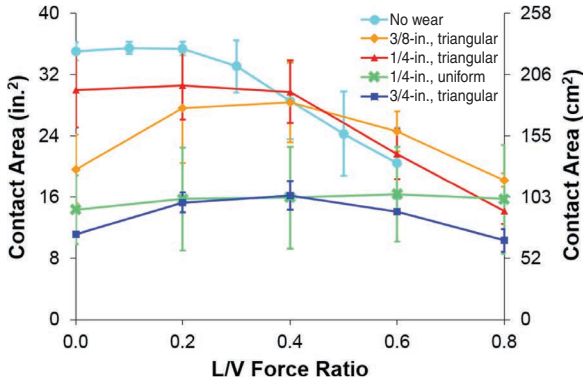

FIGURE 7 Behavior of contact area under increasing L/V at 20,000 lbf.

Figure 8 illustrates the effect of the rail seat load concentration on the pressures exerted on the rail seat. From the findings of both a literature review of rail seat load calculation methodologies and of previous field experimentation, it is assumed that half the vertical input load is transferred to the rail seat directly below the point of loading (*3*). From this assumption, it is possible to determine two primary metrics for these pressures. Figure 8*a* illustrates the average pressure for each instrumentation zone at a given L/V force ratio, which is calculated by dividing the rail seat load by the contact area (the area of the rail seat engaged in load transfer) for each rail seat and averaging all values at a given L/V force ratio. Figure 8*b* illustrates the maximum pressure observed in each instrumentation zone at a

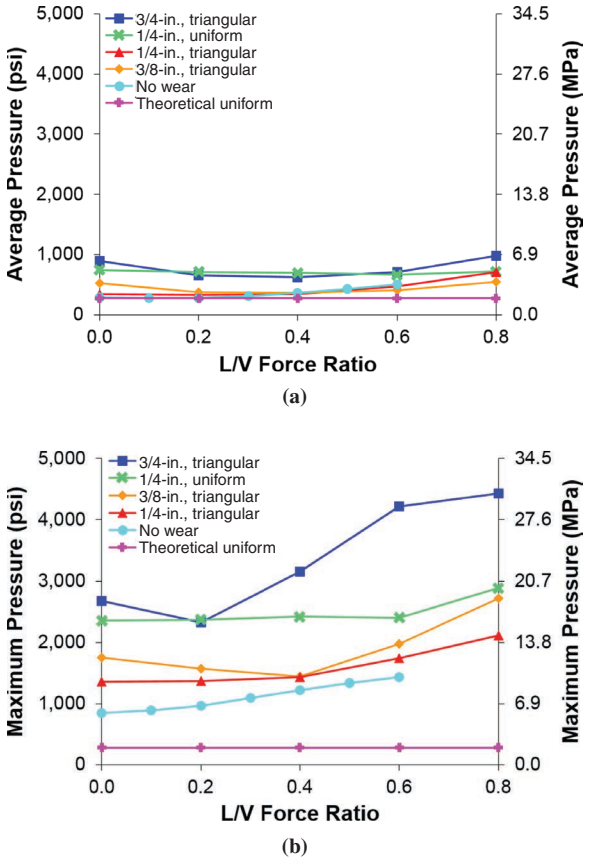

FIGURE 8 Changes in rail seat pressure under increasing L/V at 20,000 lbf: (*a*) average pressure and (*b*) maximum pressure.

given L/V force ratio. Conventional design methodology approximates the rail seat load as uniformly distributed across the entire rail seat area. This assumption is represented in Figure 8, *a* and *b*, by the data series labeled "theoretical uniform." By definition, decreased contact area correlates with increased average pressure, which is reflected in Figure 8*a*. It is immediately clear that the uniform pressure distribution does not accurately describe the behavior of the average pressure: at extreme L/V force ratios, the average pressures from even the smallest amount of RSD, the ¼-in. and ⅜-in. triangular zones, are twice the value of the uniform pressure assumption, and extreme cases of high RSD wear depth and high L/V force ratios may generate average pressures of more than 3.5 times the hypothetical uniform pressure. Moreover, Figure 8*b* shows that in the same extreme cases, the actual pressure at discrete points on the rail seat may be as much as 16 times the assumed uniform pressure. Even in areas of less severe wear, discrete points on the rail seat may experience five times the uniform pressure. The ¼-in. uniform data series yields pressures consistently higher than those of the ¼-in. triangular data series. It is hypothesized that these higher, more damaging pressures tend to alter the rail seat wear profile to one that is more similar to the triangular profile previously described.

Although the pressures shown in Figure 8 do not exceed the recommended design strength of concrete crossties, 7,000 psi (48 MPa) (*8*), the increased pressure may change the characteristics of RSD failure mechanisms such as abrasion (increased normal load will generate higher frictional forces) and hydraulic pressure cracking

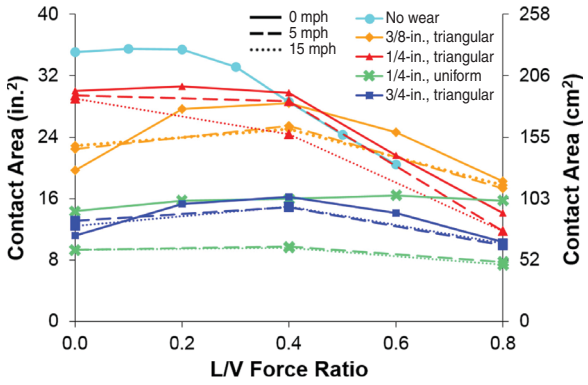

FIGURE 9 Reduction in contact area caused by dynamic load application at 20,000 lbf.

[rapid application of high pressure may produce greater tensile stresses in the concrete (*1*)]. Further, the observed pressures may be artificially lowered by restrictions of the experimental plan and its equipment. Although the T-18 was not able to apply loads simulating heavy axle freight traffic, previous research showed that the average pressure may increase by 500 psi (3.44 MPa) and that the maximum pressure can be expected to increase by 800 psi (5.52 MPa) under heavy axle loads. In addition, the artificially worn rail seats exhibited a smooth, planar surface, similar to a new and unworn rail seat. By comparison, Figure 1 shows exposed aggregate particles where the concrete paste has worn away, typical of most RSD. The less planar surface generated by field-worn RSD may further reduce the contact area, generating higher pressures than those observed in this experimentation.

Comparison of Static and Dynamic Loading

Figure 9 illustrates the effect of speed on contact area for each rail seat wear profile. Although most of the data show a reduction in contact area when the speed is increased, the data collected at 0.0 L/V show that this trend is significantly reduced or even that there is an increase in contact area with the application of speed. It is hypothesized that the lateral load may confound some dynamic effect contrary to the original hypothesis. Table 1 summarizes the relative reductions in contact area. Although experimentation with triangular wear patterns revealed a minimal effect caused by train speed, which yielded

TABLE 1 Average Reduction of Contact Area Related to Speed

Rail Seat Wear Profile	Speed (mph)	Speed (km/h)	Reduction by L/V Force Ratio (%)		
			0.0	0.4	0.8
¼-in., uniform	5	8	35	39	51
	15	24	35	40	53
¼-in., triangular	5	8	−14	10	5
	15	24	−16	12	3
⅝-in., triangular	5	8	2	4	17
	15	24	3	18	17
¾-in., triangular	5	8	−12	8	2
	15	24	−18	8	4

an average contact area reduction of 3%, experimentation at Zone 1 with the uniform wear pattern produced an average contact area reduction of 42% with the change in speed. It is hypothesized that this difference in behavior was caused by the reduced rotational restraint of the rail because of reduced or nonexistent clamping force. On average, the contact area was reduced from the static load scenario by 13% with a standard deviation of 20%. Although this does not indicate a significant effect on contact area, experimentation was constrained to relatively low speeds. In locations where trains operate at speeds two or three times greater than those tested here, this effect may be more pronounced.

Characterization of Loading Environment by Rail Cant

Figure 10 illustrates the relationship between maximum pressure and rail cant, according to data gathered from dynamic runs of the T-18 vehicle over the instrumentation zones. These data were separated by L/V force ratio and speed to isolate the effects of these variables. For rail seats with a typical 1:40 cant, FRA has established cant exception thresholds at −1.8° (alert) and −2.8° (alarm), as measured from the horizontal (*9*). These thresholds are included in Figure 10. The data indicate a trend of increasing maximum pressure with decreasing rail cant. This trend agrees with the findings previously discussed in this paper and was expected, because increased negative rail cant indicates greater rotation of the rail toward the field side, which decreases contact area. Most of the data exhibit similar trends, with the notable exception of 0.8 L/V at 5 mph, in which a consistent outlier in the data collected on rail seats with ¼-in. triangular wear has distorted the linearity of the data. The pressures observed on rail seats with no RSD at equivalent vertical loads did not exceed 1,500 psi (10.3 MPa), and a vertical load of 40,000 lbf (178 kN) generated pressures less than 2,500 psi (17.2 MPa) (*5*). At rail cants measured above the alert threshold, the maximum pressures observed at 0.8 L/V exceeded the highest pressures observed on an unworn rail seat under 40,000 lbf, which is considered to be the nominal loading case for North American heavy axle load freight service.

The relationships described in Figure 10 are quantified in Table 2, which lists the equations and R^2 values corresponding to the linear regression for each data series. If the hypothesized limit of good correlation, 0.8, is considered, then a linear correlation appears to be most suitable at low L/V force ratios. Because a GRMS typically

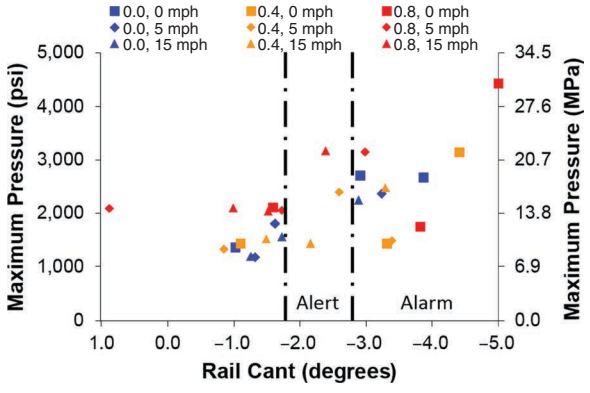

FIGURE 10 Correlation between maximum pressure and rail cant at 20,000 lbf.

TABLE 2 Linear Fit Equations for Maximum Pressure–Rail Cant Relationship

L/V Force Ratio	Speed (mph)	Speed (km/h)	Equation	R^2
0.0	0	0	$y = -500.2x + 948.0$	.877
	5	8	$y = -528.2x + 688.2$	.837
	15	24	$y = -633.9x + 419.0$	.997
0.4	0	0	$y = -443.7x + 699.7$	.572
	5	8	$y = -149.9x + 1,395$	.114
	15	24	$y = -500.2x + 948.0$	.816
0.8	0	0	$y = -572.3x + 778.9$	.462
	5	8	$y = -229.0x + 2,137$	.530
	15	24	$y = -814.0x + 1,103$	.823

operates at between 0.5 and 0.8 L/V (*10*), it is considered impractical to predict maximum pressure accurately from GRMS rail cant data on the basis of this limited data set. Correlation was improved with increased speed, but this result is inconclusive because of the limited data set. However, all instances of maximum pressures exceeding the mentioned nominal loading case for heavy axle loads on healthy track were associated with rail cants exceeding the alert threshold.

CONCLUSIONS AND FUTURE WORK

Data from this experimentation showed that the presence and severity of RSD have a significant effect on rail seat load distribution. A correlation between increased wear depth and reduced contact area was observed for triangular wear profiles; this reduction of contact area resulted in significant increases in both average and maximum pressures imparted to the rail seat, which are both drastically underestimated by conventional design methods. Also, although there did appear to be a reduction of contact area with increased speed, it was determined that the effect was negligible at low speeds or even could be reversed at low L/V force ratios. Finally, a direct correlation between rail seat load distribution and traditional GRMS measurements could not be made with the limited data collected in this experimentation. However, a general trend of maximum pressures exceeding 2,500 psi occurring only with rail cants above the FRA alert level for rail cant was observed.

A planned comparison of data from this experimentation to rail seats with field-worn RSD will better relate the findings to the field performance of concrete crossties and fastening systems. Ongoing research at UIUC is focused on the development of a framework for the mechanistic design of concrete crossties and fastening systems. As part of this effort, researchers are developing a design metric and associated methodology specifically analyzing the rail seat load distribution. The data collected from this experimentation will be useful in efforts to develop thresholds for such a metric, ultimately contributing to crosstie and fastening system designs that are inherently resistant to RSD.

ACKNOWLEDGMENTS

This research was funded by the Federal Railroad Administration, U.S. Department of Transportation and by the Transportation Technology Center (TTC). Matthew J. Greve and Marcus S. Dersch were supported by Amsted RPS. J. Riley Edwards was supported in part by

grants to the UIUC Rail Transportation and Engineering Center from the Canadian National Railway, CSX, Hanson Professional Services, and the George Krambles Transportation Scholarship Fund. The authors thank Christopher Rapp of Hanson Professional Services and Joseph LoPresti of TTC for direction, advice, and resources. The authors also thank Tim Prunkard, Don Marrow, and Matthew Csenge of UIUC for their assistance in preparing and deploying the instrumentation; Jennifer Steets of ENSCO, Inc., for providing data from the T-18; and Doug Capuder, Tiago Costa Pinto Lopes, Zachary Jenkins, and Daniel Rivi for their assistance in analyzing the data presented in this paper. Industry partnership and support were provided by Union Pacific Railroad; BNSF Railway; Amtrak; Amsted RPS/Amsted Rail; GIC; Hanson Professional Services; CXT Concrete Ties, Inc.; and TTX Company.

REFERENCES

1. Zeman, J. C. *Hydraulic Mechanisms of Concrete-Tie Rail Seat Deterioration.* MS thesis. University of Illinois at Urbana–Champaign, Urbana, 2010.
2. Van Dyk, B. J., M. S. Dersch, J. R. Edwards, C. J. Ruppert, Jr., and C. P. L. Barkan. Load Characterization Techniques and Overview of Loading Environment in North America. In *Transportation Research Record: Journal of the Transportation Research Board, No. 2448,* Transportation Research Board of the National Academies, Washington, D.C., 2014, pp. 80–86.
3. *FRA Improved Concrete Crossties and Fastening Systems for US High Speed Passenger Rail and Joint Passenger/Freight Corridors.* Railroad Transportation and Engineering Center, University of Illinois at Urbana–Champaign, 2015. http://railtec.illinois.edu/CEE/Crossties/FRA_Final_Report.php.
4. Rapp, C. T., M. S. Dersch, J. R. Edwards, C. P. L. Barkan, B. Wilson, and J. Mediavilla. Measuring Rail Seat Pressure Distribution in Concrete Crossties: Experiments with Matrix-Based Tactile Surface Sensors. In *Transportation Research Record: Journal of the Transportation Research Board, No. 2374,* Transportation Research Board of the National Academies, Washington, D.C., 2013, pp. 190–200.
5. Greve, M., M. S. Dersch, J. R. Edwards, C. P. L. Barkan, J. Mediavilla, and B. Wilson. Analysis of the Relationship Between Rail Seat Load Distribution and Rail Seat Deterioration in Concrete Crossties. *Proc., ASME Joint Rail Conference,* Colorado Springs, Colo., 2014.
6. Rapp, C. T., J. R. Edwards, M. S. Dersch, C. P. L. Barkan, B. Wilson, and J. Mediavilla. Measuring Concrete Crosstie Rail Seat Pressure Distribution with Matrix Based Tactile Surface Sensors. *Proc., 2012 ASME Joint Rail Conference,* Philadelphia, Pa., 2012.
7. Bloom, J. A., and S. Lee. The Deployable Gage Restraint Measurement System: Description and Operational Performance. *Proc., ASME Joint Rail Conference,* Pueblo, Colo., 2005.
8. *Manual for Railway Engineering.* American Railway Engineering and Maintenance-of-Way Association, Lanham, Md., 2014.
9. Clouse, A. Rail Cant Measurements of Concrete Crossties (Part 2 of 2). *Interface Journal: The Journal of Wheel/Rail Interaction,* 2008.
10. *Track and Rail and Infrastructure Integrity Compliance Manual.* Federal Railroad Administration, Washington, D.C., 2014.

The Standing Committee on Railroad Track Structure System Design peer-reviewed this paper.